2011

Simulating adsorption of U(VI) under transient groundwater flow and hydrochemistry: Physical versus chemical nonequilibrium model

Janek Greskowiak
CSIRO Land and Water

Michael Hay
U.S. Geological Survey

Henning Prommer
CSIRO Land and Water

Chongxuan Liu
Pacific Northwest National Laboratory, chongxuan.liu@pnl.gov

Vincent Post
Flinders University

See next page for additional authors

Simulating adsorption of U(VI) under transient groundwater flow and hydrochemistry: Physical versus chemical nonequilibrium model

Janek Greskowiak,[1,2] Michael B. Hay,[3] Henning Prommer,[1,4] Chongxuan Liu,[5] Vincent E. A. Post,[6] Rui Ma,[7] James A. Davis,[3,8] Chunmiao Zheng,[7] and John M. Zachara[5]

Received 13 October 2010; revised 18 March 2011; accepted 2 June 2011; published 2 August 2011.

[1] Coupled intragrain diffusional mass transfer and nonlinear surface complexation processes play an important role in the transport behavior of U(VI) in contaminated aquifers. Two alternative model approaches for simulating these coupled processes were analyzed and compared: (1) the physical nonequilibrium approach that explicitly accounts for aqueous speciation and instantaneous surface complexation reactions in the intragrain regions and approximates the diffusive mass exchange between the immobile intragrain pore water and the advective pore water as multirate first-order mass transfer and (2) the chemical nonequilibrium approach that approximates the diffusion-limited intragrain surface complexation reactions by a set of multiple first-order surface complexation reaction kinetics, thereby eliminating the explicit treatment of aqueous speciation in the intragrain pore water. A model comparison has been carried out for column and field scale scenarios, representing the highly transient hydrological and geochemical conditions in the U(VI)-contaminated aquifer at the Hanford 300A site, Washington, USA. It was found that the response of U(VI) mass transfer behavior to hydrogeochemically induced changes in U(VI) adsorption strength was more pronounced in the physical than in the chemical nonequilibrium model. The magnitude of the differences in model behavior depended particularly on the degree of disequilibrium between the advective and immobile phase U(VI) concentrations. While a clear difference in U(VI) transport behavior between the two models was noticeable for the column-scale scenarios, only minor differences were found for the Hanford 300A field scale scenarios, where the model-generated disequilibrium conditions were less pronounced as a result of frequent groundwater flow reversals.

Citation: Greskowiak, J., M. B. Hay, H. Prommer, C. Liu, V. E. A. Post, R. Ma, J. A. Davis, C. Zheng, and J. M. Zachara (2011), Simulating adsorption of U(VI) under transient groundwater flow and hydrochemistry: Physical versus chemical nonequilibrium model, *Water Resour. Res., 47*, W08501, doi:10.1029/2010WR010118.

1. Introduction

[2] The mobility of U(VI) in oxic groundwater is generally controlled by adsorption, and is regulated by solution chemistry and surface properties of the prevailing mineral phases [*Grenthe et al.*, 1992; *Kohler et al.*, 1996; *Davis et al.*, 2004; *Bond et al.*, 2008]. Nonequilibrium mass transfer processes were found to play an important role in the overall transport behavior of U(VI) at the column and field scale, especially when groundwater velocities are high [*Qafoku et al.*, 2005; *Liu et al.*, 2006; *Yabusaki et al.*, 2008; *Liu et al.*, 2008; *Liu et al.*, 2009a; *Ma et al.*, 2010]. However, surface complexation reactions of metals are known to be extremely rapid; they attain equilibrium within the order of milliseconds [e.g., *Grossl et al.*, 1997]. Thus, the nonequilibrium U(VI) mass transfer behavior observed at column and field scale is believed to result from diffusion-limited exchange between the advective mobile pore water and surface complexation sites in intragrain, intra-aggregate, and particle coating domains [*Liu et al.*, 2006; *Stubbs et al.*, 2009]. The overall U(VI) mass transfer rates are typically affected by microscopic heterogeneity in the chemical (e.g., adsorption site concentration and surface complexation thermodynamic parameters) and physical (effective diffusion coefficients and diffusion path lengths) properties of the intragrain and intra-aggregate regions.

[3] Since it is generally difficult to quantify the chemical and physical heterogeneity within the intragrain region

[1]CSIRO Land and Water, Wembley, Western Australia, Australia.
[2]Working Group Hydrogeology and Landscape Hydrology, Institute for Biology and Environmental Sciences, Carl von Ossietzky University of Oldenburg, Oldenburg, Germany.
[3]U.S. Geological Survey, Menlo Park, California, USA.
[4]School of Earth and Environment, University of Western Australia, Crawley, Western Australia, Australia.
[5]Pacific Northwest National Laboratory, Richland, Washington, USA.
[6]Flinders University, Adelaide, South Australia, Australia.
[7]Department of Geological Sciences, University of Alabama, Tuscaloosa, Alabama, USA.
[8]Lawrence Berkeley National Laboratory, Berkeley, CA 94720, USA.

0043-1397/11/2010WR010118

to allow explicitly modeling diffusion paths, a common approach is to approximate the system with a series of first-order mass transfer rates. The multirate model typically employs a distribution (e.g., gamma or lognormal) of first-order rates to describe physical diffusion processes [e.g., *Haggerty and Gorelick*, 1995, 1998; *Haggerty et al.*, 2000; *Wang et al.*, 2005]. It has often been used to simulate the nonequilibrium linear sorption of organic contaminants in porous media affected by physical and chemical heterogeneity [e.g., *Connaugthon et al.*, 1993; *Pedit and Miller*, 1994; *Chen and Wagenet*, 1995; *Culver et al.*, 1997]. Within this framework it has previously been shown that the coupled linear sorption and diffusional mass transfer between mobile pore water and microscopic immobile domains can be described by two model approaches that are mathematically equivalent [*Nkedi-Kizza et al.*, 1984; *Valocchi*, 1985; *Haggerty and Gorelick*, 1995]: the physical and the chemical nonequilibrium model. The physical model explicitly accounts for dissolved and adsorbed mass within the immobile pore domains. It treats the sorption reaction as an instantaneous process and simulates the diffusional mass exchange between mobile and immobile pore water by a set of multiple first-order mass transfer rates. The chemical model on the other hand lumps the dissolved and adsorbed mass within the immobile pore domain and simulates the nonequilibrium mass transfer by a set of multiple first-order kinetic sorption reactions. By applying a chemical multirate linear sorption model, *Qafoku et al.* [2005] could successfully describe the effect of microscale heterogeneity on the nonequilibrium adsorption/desorption behavior of U(VI) that was observed in column experiments with sediment from the Hanford 300A site, Washington, USA.

[4] As the models are based on the assumption that the sorption reactions are linear, they cannot be applied where the sorption process becomes nonlinear, e.g., for surface complexation in a dynamic environment where the local hydrogeochemical conditions can vary rapidly in space and time. Changing hydrogeochemical conditions are a common feature under field-scale conditions [*Curtis et al.*, 2006], particularly in surface water/groundwater interaction zones, such as the Hanford 300A site where the aquifer is impacted by dynamic surface water intrusion and recession due to rapid water level changes in the nearby Columbia River [*Yabusaki et al.*, 2008; *Ma et al.*, 2010; *Greskowiak et al.*, 2010]. To account for the effect of varying hydrogeochemical conditions on the U(VI) adsorption process, *Liu et al.* [2008, 2009a] substituted the linear adsorption term in the chemical nonequilibrium model by surface complexation reactions. This means the model approximates the coupled physical nonequilibrium mass transfer process (i.e., intragrain diffusion) and surface complexation reactions by a set of multiple first-order kinetics. In contrast to the corresponding physical nonequilibrium model, it eliminates explicit treatment of diffusive mass transfer and aqueous speciation within the immobile pore water of the intragrain regions. This approximation makes it computationally efficient and feasible for column [*Liu et al.*, 2008; *Yin et al.*, 2011] and field scale applications [*Ma et al.*, 2010; *Greskowiak et al.*, 2010; *Hammond and Lichtner*, 2010]. First attempts have been made to assess the chemical nonequilibrium model under variable hydrogeochemical conditions in stirred-flow reactors [*Liu et al.*, 2009a] and column experiments [*Yin et al.*, 2011], where it had produced a reasonable agreement with experimental data.

[5] The physical nonequilibrium model, however, is thought to be a more accurate representation of the kinetic regime, given the explicit inclusion of an aqueous immobile zone. This allows for differing aqueous chemistries in bulk and intragrain regions, and also has implications for mass transfer rates as a function of adsorption affinity, as we show below. Although it is the preferred model for representing a diffusive process, its implementation is often limited by its greater complexity and added computational demands. The physical model contains one additional parameter (the immobile zone porosity) and requires independent aqueous geochemical calculations for each immobile solution cell in contact with the mobile zone. The physical model can therefore easily require orders of magnitude more computational time than the chemical model, depending on model discretization. For this reason, its application even to laboratory systems can become difficult. Thus, to determine under which circumstances the chemical model is a suitable alternative to the more demanding physical model, information and understanding of how the physical nonequilibrium model responds to variable flow and hydrochemical conditions and how this compares to the behavior of the chemical nonequilibrium model under such conditions is highly important. This type of direct comparison of model predictions is currently lacking in the literature.

[6] With the present modeling study we aim to close this gap. The objectives of our investigation were to (1) characterize and compare the behavior of the chemical and physical nonequilibrium approaches to simulate coupled diffusion and equilibrium surface complexation reactions in the intragrain regions under varying hydrogeochemical conditions and its effect on macroscopic U(VI) transport behavior and (2) identify under what conditions the behavior of the chemical and the physical nonequilibrium model are expected to differ and the reasons for their divergence. The analysis was carried out for both column and field scale scenarios that reflect the characteristic hydrological and hydrogeochemical conditions at the Hanford 300A site (Figure 1).

2. Methods

[7] The simulations and subsequent analyses were carried out for a column experiment based on *Liu et al.* [2008] and a corresponding one-dimensional field scale model based on *Ma et al.* [2010] and *Greskowiak et al.* [2010]. These studies used the chemical nonequilibrium, multirate first-order kinetic surface complexation approach (see Figure 2) to account for the nonequilibrium adsorption/desorption behavior of U(VI) in the contaminated Hanford 300A aquifer.

[8] For the present study an alternative approach has been employed for comparison, i.e., the physical nonequilibrium approach that approximates diffusive mass transfer by multirate first-order solute exchange between mobile and immobile intragrain pore spaces (see Figure 2). In this physical nonequilibrium approach the U(VI) surface complexation reactions were treated as instantaneous reactions and were assumed to occur only within the intragrain porosity (see Figure 2). All flow and reactive transport simulations were performed with the groundwater flow simulator MODFLOW-2000 [*Harbaugh et al.*, 2000] and the multicomponent reactive transport model PHT3D [*Prommer*

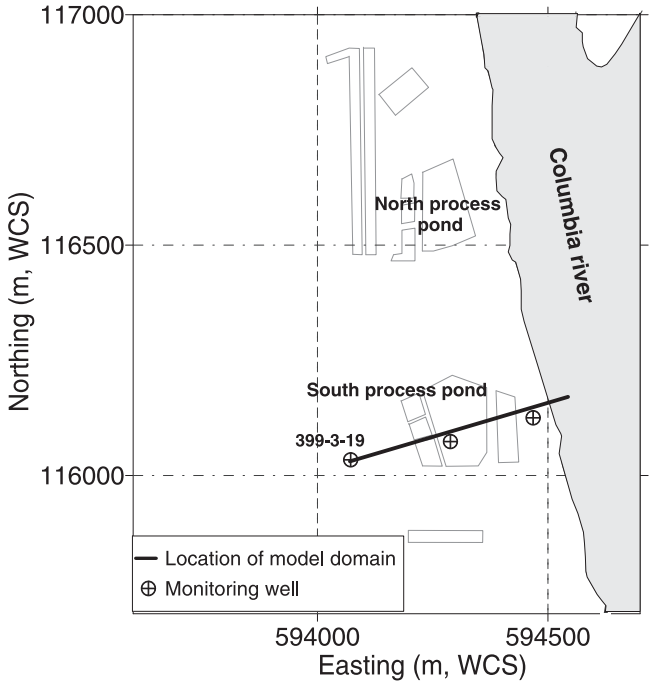

Figure 1. Hanford 300A site; location of model domain; WCS = Washington Coordinate System.

et al., 2003], respectively. PHT3D couples the multispecies transport simulator MT3DMS [*Zheng and Wang*, 1999] and the geochemical reaction model PHREEQC-2 [*Parkhurst and Appelo*, 1999] through a sequential operator splitting approach. The third-order total-variation-diminishing (TVD) method was employed for all transport simulations. It is generally highly accurate and minimizes numerical dispersion while conserving mass [*Zheng and Bennett*, 2002]. The time discretization for all reactive transport simulations has been chosen sufficiently fine to rule out numerical errors potentially induced by the temporal operator splitting technique. No redox reactions were considered in the reaction network. It was assumed that the uranium is present only in the +VI oxidation state, as the contaminated aquifer at the Hanford 300A site was found to be entirely aerobic [e.g., *Williams et al.*, 2007].

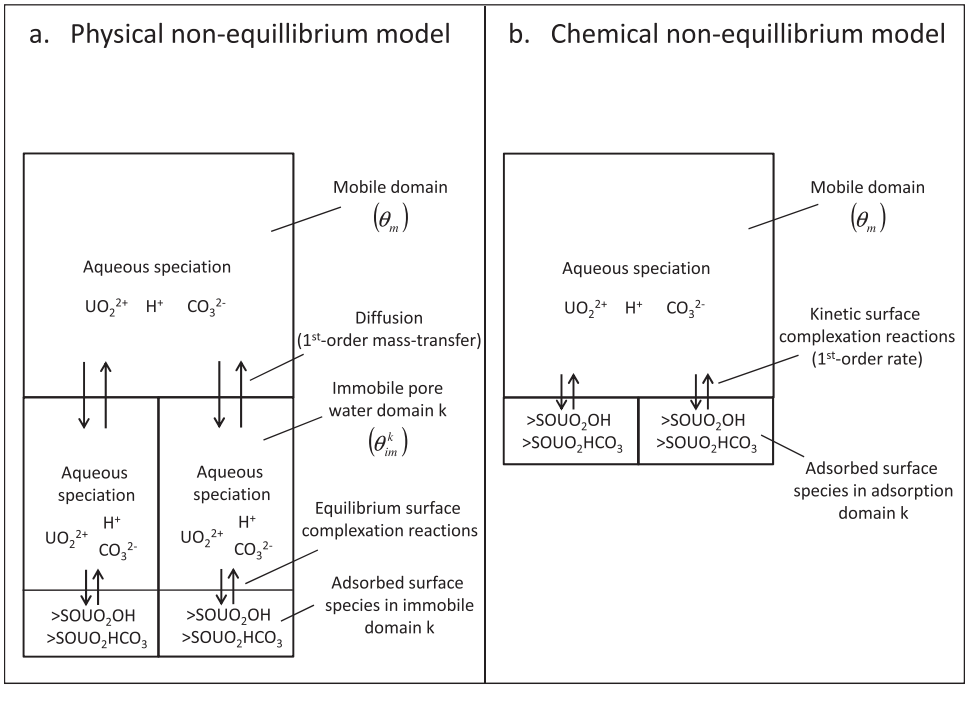

Figure 2. (a) Physical nonequilibrium approach, (b) Chemical nonequilibrium approach.

2.1. Governing Equations

2.1.1. Chemical Nonequilibrium Approach

[9] Coupling the multirate chemical kinetic surface complexation model to the one-dimensional advection-dispersion equation gives the following set of equations [*Liu et al.*, 2008]:

$$\theta_m \frac{\partial C_i^m}{\partial t} + \rho_b \sum_{j=1}^{M_i} \left(a_{ij} \sum_{k=1}^{MD} \frac{\partial m_j^{k,m}}{\partial t} \right) = \theta_m D \frac{\partial^2 C_i^m}{\partial x^2} - q \frac{\partial C_i^m}{\partial x}, \quad (1)$$

$$\frac{\partial m_j^{k,m}}{\partial t} = \alpha_k (Q_j^m - m_j^{k,m}), \quad (2)$$

with $i = 1, 2, \ldots, N$; $j = 1, 2, \ldots, M_i$; $k = 1, 2, \ldots, MD$, where C_i^m is the total aqueous concentration of chemical component i in the aqueous phase characterized by mobile porosity θ_m. Note that although we employed the chemical nonequilibrium model with only a single porosity, we label it here with the subscript m as the mobile porosity to be consistent with the formulation of the physical nonequilibrium model introduced later. ρ_b is the bulk density and $m_j^{k,m}$ (mol kg^{-1}) is the concentration of adsorbed species j in adsorption domain k; a_{ij} is the stoichiometric coefficient of chemical component i in adsorbed species j; q is the Darcy flux in one dimension, equal to the product of θ_m and the average pore water velocity ν; D is the dispersion coefficient, which is the product of longitudinal dispersivity α_L and pore water velocity ν; α_k is the chemical first-order rate constant at adsorption domain k; Q_j^m (mol kg^{-1}) is the adsorption extent of adsorbed species j and is defined as the theoretical concentration of adsorbed species j that would be in equilibrium with the aqueous phase according to the surface complexation model (see below); N is the total number of chemical components; M_i is the number of adsorbed species containing chemical component i; and MD is the total number of adsorption domains.

[10] It is assumed that the rate constants associated with the adsorption sites follow a lognormal probability distribution. In order to discretize this rate constant distribution, each adsorption domain k was assigned the same adsorption site concentration $S^k = S_{\text{tot}}/MD$, and the individual rate constants α_k were computed from [*Liu et al.*, 2008]:

$$S^k = S_{\text{tot}} \int_{\alpha_k - \frac{\Delta\alpha_k}{2}}^{\alpha_k + \frac{\Delta\alpha_k}{2}} \left[\frac{1}{\alpha\sigma\sqrt{2\pi}} \exp\left(-\frac{1}{2\sigma^2} [\ln(\alpha) - \mu]^2 \right) \right] d\alpha, \quad (3)$$

where S_{tot} is the total adsorption site concentration (mol kg^{-1}), S^k is the adsorption site concentration (mol kg^{-1}) in adsorption domain k, and μ and σ are the mean and standard deviation of $\ln(\alpha)$, respectively. For computational efficiency the number of adsorption domains was limited to $MD = 10$.

[11] The model utilized a generalized composite surface complexation model that was developed and reported earlier by *Bond et al.* [2008] for the Hanford 300A site:

$$>\text{SOH} + \text{UO}_2^{2+} + \text{H}_2\text{O} \leftrightarrow >\text{SOUO}_2\text{OH} + 2\text{H}^+ \; K_1, \quad (4)$$

$$>\text{SOH} + \text{UO}_2^{2+} + \text{CO}_3^{2-} \leftrightarrow >\text{SOUO}_2\text{HCO}_3 \; K_2, \quad (5)$$

where >SOH represents a surface site for uranyl adsorption; $>\text{SOUO}_2\text{OH}$ and $>\text{SOUO}_2\text{HCO}_3$ are the surface-complexed uranyl species; and K_1 and K_2 are the equilibrium constants for reactions (4) and (5), respectively. The adsorption extents for the surface complexes $>\text{SOUO}_2\text{OH}$ and $>\text{SOUO}_2\text{HCO}_3$ are calculated from reactions (4) and (5):

$$Q_{\text{SOUO}_2\text{OH}} = \frac{S^k \{\text{H}^+\}^{-2} K_1 \{\text{UO}_2^{2+}\}}{\{\text{H}^+\}^{-2} K_1 \{\text{UO}_2^{2+}\} + \{\text{UO}_2^{2+}\}\{\text{CO}_3^{2-}\} K_2 + 1}, \quad (6)$$

$$Q_{\text{SOUO}_2\text{HCO}_3} = \frac{S^k \{\text{CO}_3^{2-}\} K_2 \{\text{UO}_2^{2+}\}}{\{\text{H}^+\}^{-2} K_1 \{\text{UO}_2^{2+}\} + \{\text{UO}_2^{2+}\}\{\text{CO}_3^{2-}\} K_2 + 1}, \quad (7)$$

where the brackets indicate the activity of the individual aqueous species. The adsorption extents $Q_{\text{SOUO}_2\text{OH}}$ and $Q_{\text{SOUO}_2\text{HCO}_3}$ describe the theoretical surface complex concentrations of $>\text{SOUO}_2\text{OH}$ and $>\text{SOUO}_2\text{HCO}_3$ that would be present within an adsorption domain k if it was in full equilibrium with the bulk aqueous phase. Note that for the conditions of our study, including the variations in pH and carbonate concentrations, the denominator in equations (6) and (7) does not significantly deviate from 1; thus the adsorption extents are linearly proportional to the UO_2^{2+} activity. Aqueous speciation reactions were treated as equilibrium reactions and the activities of the aqueous species were calculated by the Davies equation. The stability constants of the aqueous U(VI) species were taken from *Liu et al.* [2008].

2.1.2. Physical Nonequilibrium Approach

[12] In the physical nonequilibrium model, diffusion between mobile pore water and intragrain/intra-aggregate pores is described as multirate first-order physical mass transfer [e.g., *Haggerty and Gorelick*, 1995]. The first-order mass transfer occurs between the advective (mobile) aqueous phase and MD immobile aqueous phases that reflect the intragrain and intra-aggregate regions. Coupled to a multicomponent reaction network (here aqueous speciation and surface complexation), this leads to a so-called multicomponent multicontinuum model [e.g., *Donado et al.*, 2009; *Willmann et al.*, 2010]. For one-dimensional advection-dispersion it is described by the following set of equations:

$$\theta_m \frac{\partial C_i^m}{\partial t} + \sum_{k=1}^{MD} \left(\theta_{im}^k \frac{\partial C_i^{im,k}}{\partial t} + \rho_b \sum_{j=1}^{M_i} b_{ij} \frac{\partial p_j^{im,k}}{\partial t} \right) = \theta_m D \frac{\partial^2 C_i^m}{\partial x^2} - q \frac{\partial C_i^m}{\partial x}, \quad (8)$$

$$\theta_{im}^k \frac{\partial C_i^{im,k}}{\partial t} + \rho_b \sum_{j=1}^{M_i} b_{ij} \frac{\partial p_j^{im,k}}{\partial t} = \omega_k \theta_{im}^k (C_i^m - C_i^{im,k}), \quad (9)$$

with $i = 1, 2, \ldots, N$; $j = 1, 2, \ldots, M_i$; $k = 1, 2, \ldots, MD$, where C_i^m (mol L^{-1}) is the total aqueous concentration of chemical component i in the mobile domain, $C_i^{im,k}$ is the total aqueous concentration of chemical component i in the pore water of immobile domain k, $p_j^{im,k}$ (mol kg^{-1}) is the concentration of adsorbed species j in immobile domain k, θ_m is the mobile porosity, θ_{im}^k is the porosity in immobile domain k, b_{ij} is the stoichiometric coefficient of chemical

component i in adsorbed species j, ω_k is the physical first-order rate constant between the mobile domain and immobile domain k, and M_i is the number of adsorbed species.

[13] The absorbed equilibrium concentrations $P_j^{im,k}$ in the physical model are calculated from the surface complexation reactions (equations (4) and (5)) depending on the aqueous species concentrations and the surface site density S^k in each immobile domain. The total immobile porosity θ_{im} is the sum of the individual immobile porosities θ_{im}^k. The total immobile porosity was set to $\theta_{im} = 8 \times 10^{-4}$ for all simulations (Table 2), based on grain fracture porosities found for vadose zone sediments from the Hanford BX tank farm [*Ilton et al.*, 2008; *Liu et al.*, 2009b].

[14] In the physical nonequilibrium model we assumed that the physical rate constants associated with the immobile porosities follow a lognormal probability distribution, where the rate constant for each of the immobile domains can be computed from

$$\theta_{im}^k = \theta_{im} \int_{\omega_k - \frac{\Delta\omega_k}{2}}^{\omega_k + \frac{\Delta\omega_k}{2}} \left[\frac{1}{\omega\sigma\sqrt{2\pi}} \exp\left(-\frac{1}{2\sigma^2} [\ln(\omega) - \mu]^2 \right) \right] d\omega, \quad (10)$$

where μ and σ are the mean and standard deviation of $\ln(\omega)$, respectively. Corresponding to the discretization procedure for the chemical nonequilibrium model, 10 immobile domains and associated physical rate constants were used in this study, and each of the immobile domains was assigned the same immobile porosity $\theta_{im}^k = \theta_{im}/MD$. As information about the relation between sorption site density S^k and the immobile porosity θ_{im}^k of an immobile domain k is typically not readily available, we assumed for simplicity that the sorption site density is uniformly distributed across the immobile domains: $S^k = S_{tot}/MD$, and thus is consistent with the chemical nonequilibrium model.

2.2. Column Scenarios

[15] The column scenarios were adapted from earlier simulations of a large column experiment with U(VI) contaminated Hanford 300A field textured sediment [*Liu et al.* 2008]. The 80 cm column was flushed with a synthetic groundwater solution to investigate U(VI) desorption behavior. On the basis of the original experiment and simulations of *Liu et al.* [2008], we introduced a hypothetical case with varying hydrochemical composition of the inflow solution to reflect the hydrochemical dynamics of groundwater-river water mixing that occurs at the Hanford 300A site. The solutions for the column simulations were selected to correspond to the hydrochemical end members observed in the field, which include the average Columbia River water and the average ambient groundwater (Table 1). The ambient groundwater is characterized by a lower pH and higher carbonate and calcium concentrations and thus, according to the proposed site specific surface complexation model (equations (4) and (5)), leads to a lower U(VI) adsorption affinity than the river water, which has a higher pH and lower carbonate and calcium concentrations [*Ma et al.*, 2010; *Greskowiak et al.*, 2010].

[16] The Hanford 300A U(VI) plume exhibits complex hydrologic and hydrochemical behaviors because of its linkage with the Columbia River that experiences daily (~1 m) and seasonal (~2.5 m) stage changes. During the low river flow period (August–April), groundwater flows primarily toward the river, and daily river stage changes cause brief periods of river water intrusion that extend 10–20 m inland. River stage oscillations over this period cause frequent changes in groundwater flow direction. In the spring and early summer (April–August), the river stage increases by up to 3 m causing an extended period of river water intrusion that may extend as much as 150 m inland. River stage oscillations over this period continue to cause short term changes in groundwater flow direction. The period of high water ends gradually in late July and August, with an oscillating mixing zone of groundwater and river water that moves slowly from west (inland) to the river boundary.

Table 1. Aqueous Composition of Initial and Inflow Solutions[a] (mol L^{-1})

Component	Groundwater Average Values From 42 Wells in Hanford 300A	River Average Values During 2001–2007 at Richland WA (USGS)
pH	7.303	7.8
pe	1.5	1.5
Na	1.035×10^{-3}	1.006×10^{-3}
Ca	1.206×10^{-3}	4.495×10^{-4}
Mg	5.097×10^{-4}	1.823×10^{-4}
SO_4^{-2}	6.379×10^{-4}	9.250×10^{-5}
NO_3^-	4.700×10^{-3}	8.000×10^{-6}
TIC[b]	2.574×10^{-3}	1.128×10^{-3}
Cl[c]	5.305×10^{-4}	9.288×10^{-5}

[a]Except pH and pe, note that the pe has no effect in the present models as no redox reactions were simulated.
[b]Total dissolved inorganic carbon.
[c]Chloride used for charge balancing required by PHT3D.

[17] To evaluate these characteristic field conditions with respect to the behavior of the physical and chemical nonequilibrium model approaches, two column scenarios were investigated. In both scenarios the initial pore water solution at $t = 0$ was set to the composition characterizing groundwater. Subsequently, the model columns were flushed with groundwater and with alternating groundwater and river water in scenarios C1 and C2, respectively. C1 (constant chemistry) is the constant inflow of groundwater. C2 (variable chemistry) is the alternating inflow of groundwater and river water starting with groundwater.

[18] First, the chemical nonequilibrium model was employed for both scenarios with the chemical rate constant distribution as used in previous studies [*Liu et al.*, 2008; *Ma et al.*, 2010; *Greskowiak et al.*, 2010]. Then, with the physical rate constant distribution parameters calculated as described below, the physical model was employed for scenarios C1 and C2. This procedure reflects situations where the models were calibrated for constant hydrochemical conditions (e.g., groundwater) but later applied under more variable hydrochemical conditions (variable mixes of river water and groundwater).

[19] U(VI) was assumed to exist solely in the adsorbed state at the beginning of the simulation ($t = 0$) for the column scenarios. Flushing with a U(VI) free solution started after an initial equilibration time of approximately 3 days. The inflow rate was held constant, with several flow interruptions by stop flow events. These were introduced to

Table 2. Parameters of Column and Field Scale Models

Parameter	Value	Unit	Description
q, k_f[a]	0.27, 7000	m d^{-1}	Darcy flux, hydraulic conductivity
θ_m	0.266	–	mobile porosity
θ_{im}[b]	8×10^{-4}	–	immobile porosity
δ_b	1.945	kg L_{bulk}^{-1}	bulk density
α_L	0.11,[c] 2.0[a]	m	Longitudinal dispersivity
$\log K_1$	−4.42	–	logarithm of equilibrium constant (equation (4))
$\log K_2$	16.53	–	logarithm of equilibrium constant (equation (5))
S_{tot}^{bulk}	0.0126	mol L_{bulk}^{-1}	total bulk sorption site density
U_{tot}^{bulk}	7.72×10^{-6}	mol L_{bulk}^{-1}	total bulk initial uranium concentration
μ	−9.96,[d] 0.39[b]	ln(h^{-1})	mean of natural logarithm of the rate constant distribution
σ	2.68	ln(h^{-1})	Standard Deviation of natural logarithm of the rate constant distribution
MD	10	–	number of sorption/immobile domains (equal to number of rates)

[a]For the field scale simulations only.
[b]Only for the physical nonequilibrium model.
[c]For the column simulations only.
[d]Only for the chemical nonequilibrium model.

discern between the individual processes of nonequilibrium U(VI) release and transport by advection-dispersion. The timing and the duration of the stop flow events were identical to those of the column experiments and simulations described by *Liu et al.* [2008] and *Greskowiak et al.* [2010]. All model parameters in the physical and chemical nonequilibrium models are given in Table 2.

2.3. Field Scale Scenarios

[20] The field scale scenarios employed in this study resembled those studied by *Ma et al.* [2010] and *Greskowiak et al.* [2010]. Following *Greskowiak et al.* [2010], a one-dimensional model was utilized to represent the highly permeable upper Hanford formation. The model domain is positioned in an east-west direction adjacent to the Columbia River (Figure 1). The extent of the model domain was 500 m and its flow boundaries were set as time-variant, constant head boundaries. The western (inland) boundary was defined by hourly hydraulic head data observed at monitoring well 399–3-19 (Figure 1). The river side boundary was defined by hourly hydraulic head data extracted from a calibrated cross-sectional model of this site developed by *Ma et al.* [2010]. The inflow solution at the western (inland) boundary was defined as the ambient groundwater (Table 1), while that at the river side boundary was set as river water (Table 1). The initial conditions in the entire model domain were defined as the ambient groundwater composition (Table 1). The simulation time was one year from 27 October 2007 to 27 October 2008. The initial U(VI) plumes in the aqueous phase were created by placing all U(VI) into the sorbed phase following an initial equilibration time of 5 days under no-flow conditions. This allowed for an almost complete equilibration with the aqueous phase. In order to assess how different assumptions on the initial conditions with respect to the location and extent of the U(VI) plume would affect the results of the physical and chemical nonequilibrium models, three field scale scenarios F1–F3 were investigated.

[21] In scenario F1, the U(VI) plume is initially ($t = 0$) present between 300 and 340 m from the western boundary, such that it is located well within the furthest reach of seasonal river water intrusion (similar to the model setup in *Greskowiak et al.* [2010]).

[22] In scenario F2, the U(VI) plume is initially present between 200 and 480 m from the western boundary and thus covers both the zone of marginal influence of river water intrusion distant from the river and the zone of dominant groundwater–surface water mixing close to the river.

[23] In scenario F3, the same as scenario F2 but the initial U(VI) plume is extended eastward such that its edge is located directly adjacent to the river side boundary. This means that in contrast to scenario F2 there is no initial U(VI)-free zone between the eastern edge of the initial plume and the river side boundary.

[24] All field scale scenarios were carried out for the chemical and physical nonequilibrium model utilizing the respective rate constant distribution parameters from the column scenarios. This reflects the situation where the models would have been calibrated from field data of an U(VI) sorption/desorption experiment carried out under strict groundwater conditions, e.g., at a location or during a time period where this location is not affected by river water intrusion. This is indeed a likely scenario as, e.g., in the current Hanford 300A integrated field scale research challenge (IFRC) project of the US Department of Energy, the high resolution grid of monitoring wells for field scale tracer and adsorption/desorption experiments was installed at a location 120 m from the river shoreline that is affected by river water intrusion approximately every second or third year. The physical and chemical nonequilibrium models were compared for the simulated U(VI) concentration profiles in the model domain and for U(VI) mass flux to the river.

3. Results and Discussion

3.1. Physical and Chemical Model Comparison Under Linear Sorption

[25] Before presenting the calculation results obtained for the column and field scenarios, it is useful to compare the physical and chemical model formulations side-by-side to understand how the two models behave and under what circumstances they would be expected to deviate. For this purpose, simplification to linear-adsorption formulations of the models serves as a more convenient starting point. It is important to note that for the conditions of our study, the linear adsorption (K_d) concept can indeed be utilized to

explain and compare the behavior of the two nonequilibrium models under the considered scenarios. This is because (1) adsorption occurs far from saturation of the adsorption sites for the considered surface site and U(VI) concentrations and (2) the activity of aqueous species UO_2^{2+} is approximately linearly proportional to the total U(VI) component concentration and to the adsorbed concentration (see section 2.1). Thus, adsorption/desorption of U(VI) can be described with the constant K_d linear sorption model if the water chemistry is not varying. When the water chemistry is varying, the value of the linear distribution coefficient K_d mainly depends on the pH and the carbonate and calcium concentrations as a result of the surface complexation reactions. Therefore, the K_d varies for different mixing ratios of river water and groundwater (Figure 3). The K_d does not change linearly with the mixing ratio, as the mixing of these two different water types leads to nonlinear changes in aqueous speciation which, in turn, lead to nonlinear effects on surface complexation.

[26] A comparison of physical and chemical nonequilibrium linear adsorption model formulations was performed by *Nkedi-Kizza* [1984] for a single rate-limited immobile domain. Equivalence of these two models in a multirate context was demonstrated in the work of *Haggerty and Gorelick* [1995]. This means it is possible to convert between the rate constants of the chemical and the physical model. Following *Haggerty and Gorelick* [1995], the conversion can be obtained assuming that (1) the mass of dissolved U(VI) in the immobile zone is very small compared to the mass of adsorbed U(VI) at any given time (which is the case in our study due to the extremely small amount of immobile pore water) and (2) the sorption site densities are uniformly distributed across the sorption/immobile domains of the model (the derivation is given in the auxiliary material):

$$\mu_{\text{physical}} = \mu_{\text{chemical}} + \ln\left(\frac{\rho_b K_d}{\theta_{im}}\right), \tag{11}$$

where K_d (L kg^{-1}) is the distribution coefficient for U(VI), μ_{physical} and μ_{chemical} are the logarithm mean of the rate constant distribution of the physical and chemical model, respectively.[1] Note that the standard deviation of the rate constant distribution will be identical for the physical and chemical model.

[27] From equation (11), one can calculate for a specific K_d a logarithm mean of the physical rate constant distribution so that the physical model produces the same simulation results as the chemical model. However, when the K_d changes in response to variations in water chemistry, the physical and chemical model formulations will subsequently predict different kinetic behavior. For instance, a reduction in adsorption strength (decrease in K_d) due to water chemistry changes would result in an enhanced mass transfer rate in the physical model relative to the chemical model, whereas an increase in adsorption strength would result in a slower mass transfer rate in the physical model. The transport of U(VI) will consequently be influenced in different ways depending on aqueous chemistry and flow, as illustrated in the modeling results of the column and field-scale scenarios discussed below.

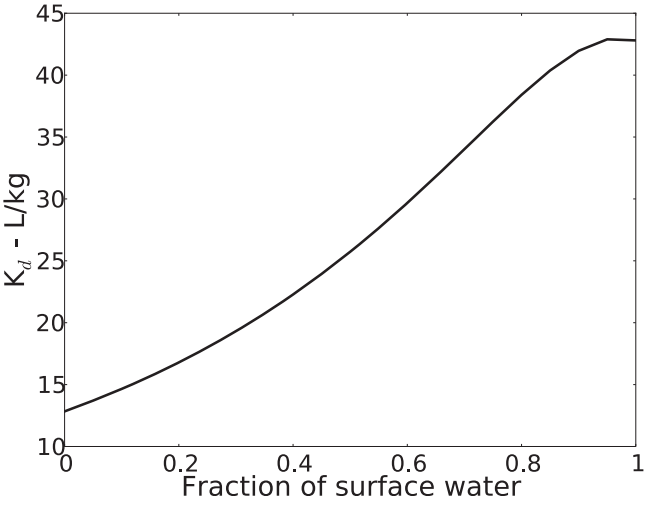

Figure 3. K_d for U(VI) as a function of surface water–groundwater mixing ratio, calculated from the surface complexation reactions (4) and (5) and the surface site concentration given in Table 2.

3.2. Column Scenarios

3.2.1. Constant Water Composition

[28] The injection of a constant water composition into the column was simulated in scenario C1 representing typical groundwater. After the initial equilibration time of 3 days, a U(VI) free solution was pumped into the column that caused a sudden decrease in the simulated U(VI) concentration at the outlet of the column (Figure 4). Comparable decreases were observed after each of the stop flow events (Figure 4). The decrease occurred because U(VI) could not be desorbed quickly enough during the residence time to maintain the high concentration levels generated during either initial equilibration or the stop flow events. The U(VI) concentration increases and the system slowly approaches adsorption equilibrium during the stop flow events. In contrast, the flushing phases are characterized by strong adsorption disequilibrium as the concentration difference between adsorption extent and the actual adsorbed concentrations (in the chemical nonequilibrium description) is maintained due to the U(VI) free solution entering the column. Note that the term "adsorption disequilibrium" will also be used in discussions of the physical nonequilibrium model where the mobile and immobile pore water are not in equilibrium with respect to the U(VI) concentrations. A comprehensive description and discussion of the processes observed in the experiment, including multirate kinetics, can be found in *Liu et al.* [2008] and *Greskowiak et al.* [2010].

[29] As outlined in the previous section, sorption of U(VI) can be considered as linear for a given water composition. Thus, in order to obtain identical simulation results of the physical and the chemical nonequilibrium model for groundwater conditions in scenario C1 (Figure 4), the logarithm mean of the physical rate constant distribution was adjusted after equation (11) utilizing a K_d of 12.8 L kg^{-1} (Figure 3). The calculated logarithm mean for the physical

[1] Auxiliary materials are available in the HTML. doi:10.1029/2010WR010118.

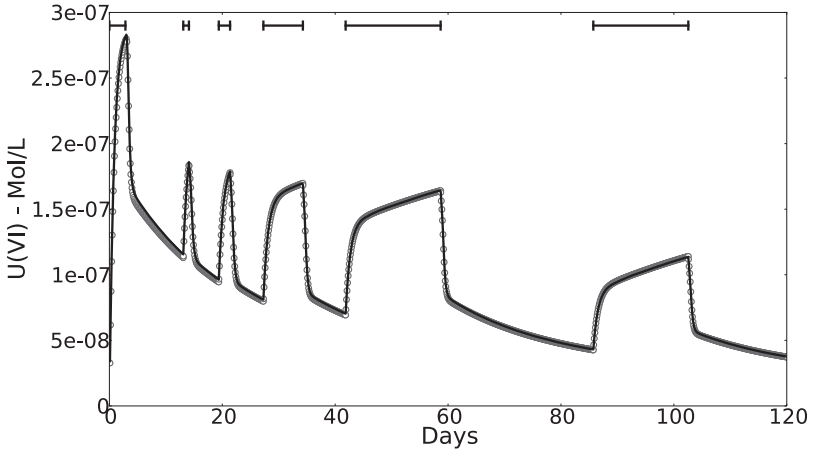

Figure 4. U(VI) concentration versus time at the outlet end of the column for scenario C1 (constant chemistry) simulated with the chemical (line) and physical (circles) nonequilibrium model; horizontal bars indicate time and duration of stop flow events.

model is given in Table 2. As expected, the physical and chemical models yield identical results under constant aqueous chemical conditions (Figure 4).

3.2.2. Variable Water Composition

[30] We had calculated the logarithm mean of the rate constant distribution of the physical model to reproduce the simulation results of the chemical nonequilibrium model under scenario C1 (Figure 4). Now both the chemical and physical nonequilibrium models were exposed to variable chemical conditions, as defined in scenario C2, while their rate constant distribution parameters were not changed.

[31] River water was injected into the column in scenario C2 after the initial equilibration with groundwater. The sudden drop in effluent U(VI) concentration was more pronounced with river water than it was with groundwater (Figure 5). A comparable response was noted for both the chemical and physical nonequilibrium models, and resulted from the higher adsorption strength associated with river water composition (Figure 3). This behavior was observed for all cases where the inflow water composition was changed to river water. As explained in section 3.1, the mass transfer rate and the kinetic adsorption rate of the physical and chemical model, respectively, do not change in the same way with changing K_d. For example, with a change from groundwater to river water and thus increasing K_d (Figure 3), the rates in the chemical model would increase in comparison to the physical model. Thus, after the switch to river water in scenario C2, desorption rates are higher and the drop of U(VI) concentrations is not as pronounced for the chemical model as for the physical model.

[32] As the different behavior of the chemical and physical nonequilibrium model under changing water composition (or changing actual K_d) is a result of the different impacts on the kinetic and mass transfer rates, respectively, the effect is stronger when the adsorption disequilibrium is higher. On the other hand, when the system approaches equilibrium, e.g., during the stop flow events, the discrepancy between the chemical and physical nonequilibrium model decreases,

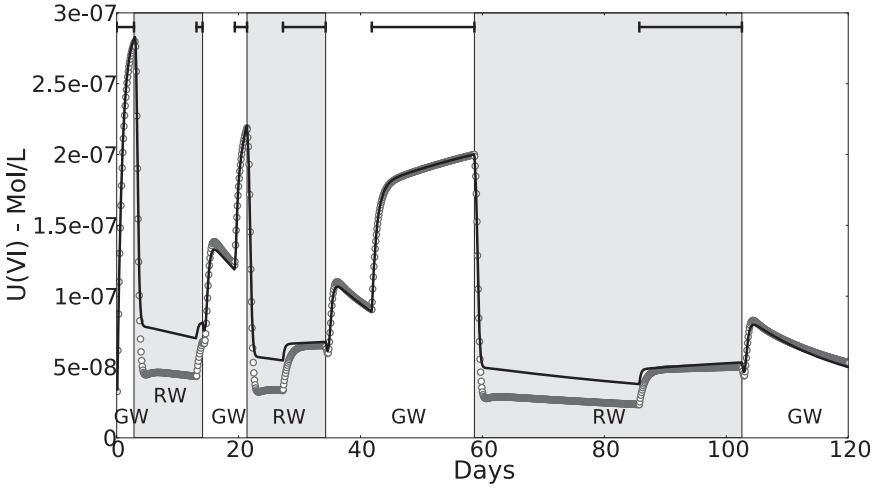

Figure 5. U(VI) concentration versus time at the outlet end of the column for scenario C2 (variable chemistry) simulated with the chemical (line) and physical (circles) nonequilibrium model; white area corresponds to groundwater (GW) injection period and gray shaded area corresponds to river water (RW) injection period; horizontal bars indicate time and duration of stop flow events.

as can be seen for the longer stop flow periods, e.g., between 28 and 35 days (Figure 5).

[33] The different behavior of the chemical and physical model under changing water composition is clearly noticeable in our column simulations; the relative difference is always around 50% under river water conditions. *Yin et al.* [2011] showed that U(VI) desorption data from column experiments assigning hydrochemically changing inflow solutions could be moderately well described with the chemical nonequilibrium model. Experimental uncertainties, especially uncontrolled water chemistry changes from buffering reactions, mainly calcite dissolution, within the column were assumed to be the main reason for the discrepancy of experimental data and simulation. They concluded that processes affecting the major ion chemistry largely controlled the adsorption/desorption behavior of U(VI) rather than mass transfer rates. To test whether calcite dissolution has a mitigating effect on the different behavior of the two models under changing inflow chemistry, we have carried out an alternative column scenario. In this scenario, calcite has been allowed to dissolve. Calcite started to dissolve when the calcite undersaturated river water entered the column. This resulted in an increasing pH as well as increased carbonate and calcium concentrations in the river water and lowered the associated K_d from ~43 L kg^{-1} (see Figure 3) to 24 L kg^{-1}, which is closer to the K_d of ~13 L kg^{-1} associated with groundwater (Figure 3). Therefore, the relative difference between the simulation results of the two nonequilibrium models decreased to around 25% under river water conditions (simulation results not shown).

[34] Another interesting, although small effect is unique to the physical nonequilibrium model. After each concentration drop caused by the flushing with river water in scenario C2, the U(VI) concentrations increase slightly within the following 1–2 days until they gradually start to decrease for the rest of the flushing phase. An illustrative PHREEQC batch-type simulation provides insight into why this phenomenon occurs. In this simulation the immobile domains and their adsorption sites were initially set to be in equilibrium with groundwater (i.e., aqueous U(VI) in the immobile pore water is 3 μmol L^{-1}), while the mobile pore water was assumed to be river water containing a lower U(VI) concentration (0.09 μmol L^{-1}). This represents a situation encountered when the first pore volume of river water has just reached the outlet of the column that was in previous contact with groundwater. With the river water present in the mobile domain, mass transfer leads to a gradual change in the chemistry of the immobile pore water from groundwater to river water: pH increases and carbonate and calcium concentrations decrease, thus increasing adsorption potential. This triggers surface complexation of U(VI) in the immobile pore, with concomitant proton release. The displaced protons affect the pH in the volumetrically small immobile domains (Figure 6a), decreasing from 7.3 to 7.15. Associated changes in aqueous carbonate, calcium, and UO_2^{2+} speciation occur and lead to an order of magnitude increase in adsorption strength (or the actual K_d) for U(VI) (Figure 6b). The resulting decrease in U(VI) aqueous concentrations in the immobile pore water (Figure 6c) increases the U(VI) flux from the mobile into the immobile domains, and decreases U(VI) concentrations in the mobile domain (Figure 6d).

[35] The amplified adsorption in the immobile domains eases when the river water pH becomes dominant in the immobile pore water causing a reduction in adsorption strength (or actual K_d) back to the value associated with river water (Figure 6b). U(VI) concentrations in the immobile domains consequently increase again (Figure 6c) such that the direction of flux changes, and U(VI) is transferred

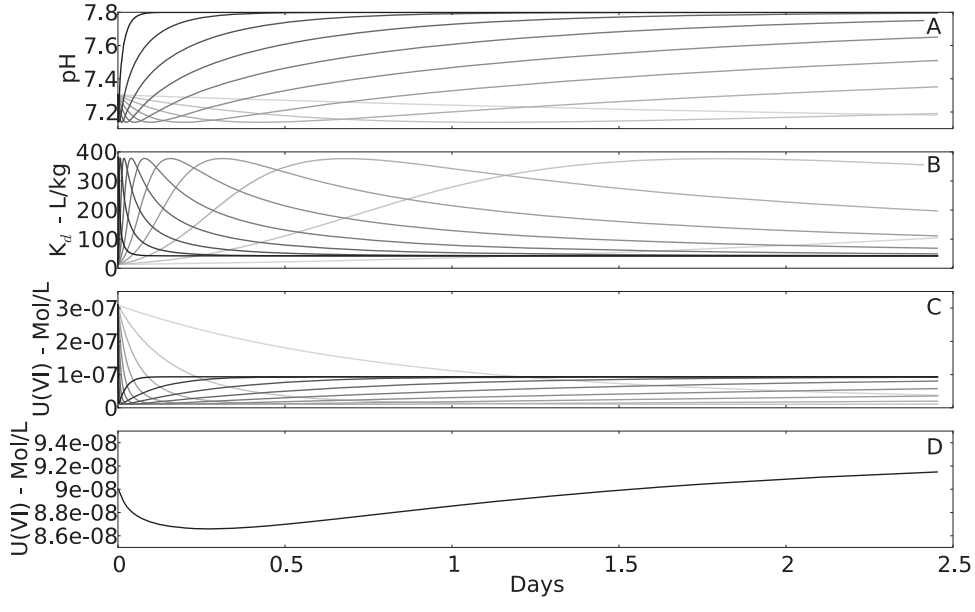

Figure 6. PHREEQC batch calculation of the physical nonequilibrium model, after switching from groundwater to river water in the mobile domain. (a) Evolution of pH, (b) actual K_d, and (c) U(VI) concentration in the pore water of the immobile domains, where the darker color represent the domains with a higher mass transfer constant and the lighter color represent the domains with a lower mass transfer constant. (d) Evolution of the U(VI) concentration in the mobile pore water.

back to the mobile domain (Figure 6d). This means that the effect of amplified adsorption strength occurs only at early times of river water contact. Consequently, a water parcel entering the column at the beginning of the river water injection period would not become as quickly enriched by desorbing U(VI) as water parcels entering the column during later times of river water injection, resulting in decreased U(VI) concentrations at the leading edge of the river water plume. This effect is not noticeable for the chemical nonequilibrium model because the protons released by U(VI) surface complexation are released directly into the mobile zone where they are diluted to insignificance. Although the influence of the pH excursion is relatively small, they illustrate how transient differences in mobile and immobile zone chemistry can affect U(VI) speciation and kinetics; effects not captured by the chemical model.

[36] When the injection water in scenario C2 was switched back to groundwater, the simulated U(VI) concentration increased again due to the lower K_d generated by the groundwater composition (Figure 5). The U(VI) concentration becomes even higher than in scenario C1 because of the different mass removal histories of U(VI) from adsorption sites in the two scenarios. The mass removal of U(VI) by river water in scenario C2 was less than by groundwater because of the higher adsorption potential in river water. More U(VI) is then available for desorption in scenario C2 when groundwater is reintroduced than it is in scenario C1. This leads to higher effluent concentrations in scenario C2.

3.3. Field Scale Scenarios

3.3.1. Dynamics of the U(VI) Plume

[37] A range of field scale scenarios was simulated to evaluate physical and chemical nonequilibrium behavior with respect to different initial U(VI) plume locations and extents. The corresponding rate constant distribution parameters were the same as those utilized in the column scenarios. The principal behavior observed for both the physical and chemical nonequilibrium model was that only limited plume movement occurs after the initial 5 day equilibration period, as shown for scenarios F1 and F2 in Figure 7 (note that day zero in Figure 7 is after the initial 5 day equilibration period). This is a result of the combined effect of chemically induced retardation and 1–3 groundwater flow direction reversals per day, slowing down plume migration. Note that the annually averaged Darcy velocity is 0.2 m d^{-1} toward the Colombia River. Uncontaminated water from the plume fringes does not intrude quickly and far enough into the plume as a result of the daily groundwater flow reversals to generate strong adsorption disequilibrium, except during short time periods of fast and sustained unidirectional flow [*Greskowiak et al.*, 2010; *Hammond and Lichtner*, 2010]. The plume center is predominantly characterized by near-equilibrium conditions, while the plume fringes are dominated by strong sorption disequilibrium [*Greskowiak et al.*, 2010]. This can be seen from the mass transfer rates, e.g., bulk adsorption/desorption rates of the chemical nonequilibrium model shown for scenarios F1 and F2 in Figure 7. Higher rates indicate a higher degree of sorption disequilibrium.

[38] When the river water comes in contact with the U(VI) plume during river water intrusion periods (indicated by the pH profiles in Figure 7), U(VI) concentrations decrease as a result of stronger adsorption promoted by the river water composition. This behavior occurs in scenario F1 only during the spring high water stage where river water intrudes far into the aquifer (e.g., between 216 and 264 days; see Figure 7). U(VI) concentrations increase again after river water recedes and is replaced by ambient groundwater (Figure 7). The gradual decrease of U(VI) concentration in the plume center during the simulation period, however, is due to dispersive spreading of the plume. A temporal decrease of U(VI) concentrations in the region of the plume located closest to the river occur at a high frequency during the simulation period for scenarios F2 and F3 (shown for scenario F2 only), as river water in this zone intrudes and recedes on a daily, sometimes hourly frequency.

[39] The easterly edge of the initial plume (day zero) in scenario F2 is located 20 m away from the river. During times when the groundwater flow direction points toward the river (Figure 7), U(VI) is transported from the plume center into the region where adsorbed U(VI) was initially absent (i.e., between initial plume edge and river). Dissolved U(VI) adsorbs to surface sites in that region. Aqueous U(VI) that passes this zone is discharged to the river.

3.3.2. Chemical Versus Physical Nonequilibrium Model

[40] The U(VI) plume behaves similarly for both the chemical and physical nonequilibrium models, as shown for scenarios F1 and F2 in Figure 7. Small differences in U(VI) concentrations can be observed at locations where two conditions are fulfilled at the same time: (1) the plume is affected by river water intrusion, i.e., exposed to water composition changes (Figure 7) and (2) the system is in adsorption disequilibrium. This is in agreement with the findings from the column simulations.

[41] Concentration differences between the two models were only observable for scenario F1 when river water has intruded far into the aquifer, approximately 200 and 290 days after the start of the simulation (Figure 7). At day 264, i.e., the beginning of river water recession, groundwater movement has occurred toward the river during the previous 24 h and a groundwater–river water mixture has reached the plume area from the west (see pH in Figure 7). Enhanced desorption occurs as a result of the associated decrease in K_d. However, mass transfer is slower for the physical nonequilibrium model because the actual K_d in the plume is still higher than that in the ambient groundwater. Desorbed U(VI) concentrations are accordingly lower during desorption near the center of the plume. On the other hand, adsorption occurs at the downstream side of the plume as U(VI) is transported to largely unoccupied adsorption sites in the plume fringe. Adsorption occurs more slowly for the physical nonequilibrium model than for the chemical model, leaving higher U(VI) concentrations in the fringe zone downstream of the plume.

[42] In scenario F2, when the groundwater is flowing toward the river but the hydrochemical environment is still dominated by river water conditions (e.g., days 72, 96, 240, 264, and 288) the U(VI) concentrations of the chemical nonequilibrium model at the plume fringe (i.e., between initial plume edge and river) are lower than those of the physical nonequilibrium model. Here the same explanation holds as for scenario F1; the fringe zone is affected by a higher K_d compared to the case where ambient groundwater

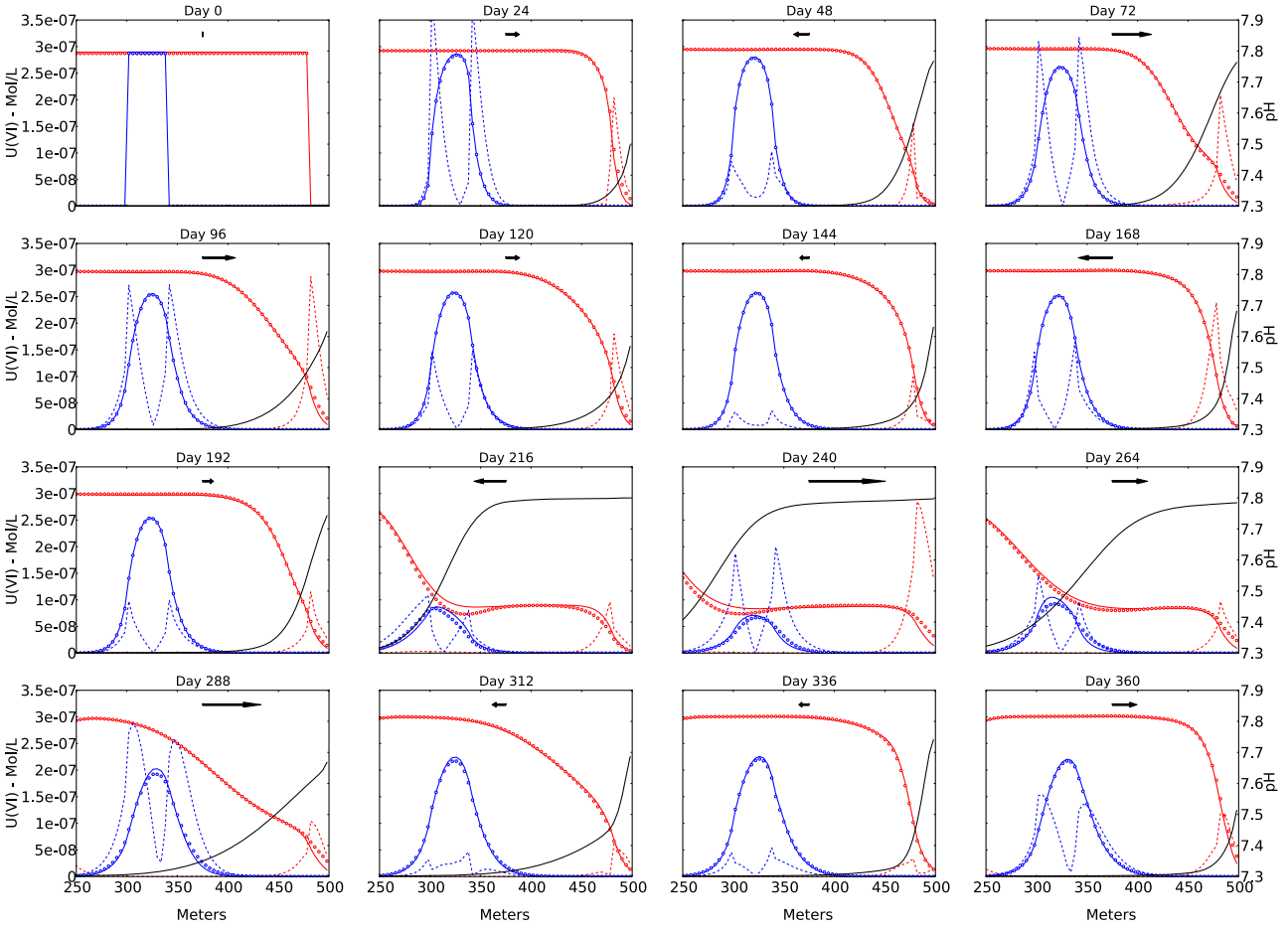

Figure 7. U(VI) concentration profiles in the mobile pore water along the model domain for field scale simulations in scenario F1 (blue) and scenario F2 (red) with the chemical (solid lines) and the physical nonequilibrium model (circles) at different simulation times. pH profiles (black solid line) indicate the extent of river water intrusion. The river side boundary is located at 500 m. The red and the blue dashed lines indicates the absolute U(VI) adsorption/desorption rate (mmol L^{-1} h^{-1} at the left axis) of the chemical nonequilibrium model in scenarios F1 and F3, respectively. Note that only the section between 250 and 500 m of the model domain is shown here. The groundwater flow direction and its magnitude (averaged over 24 h) is indicated by the arrows. Day 0 is defined after the initial 5 day equilibration period.

conditions were present, leading to higher adsorption rates in the chemical nonequilibrium model. Therefore, more U(VI) mass leaves the aquifer in the physical nonequilibrium model (Figures 7 and 8). For the same reason, when the groundwater flow is directed inland and the hydrochemical environment is dominated by river water, e.g., at day 216, the uncontaminated river water in the physical nonequilibrium model does not become enriched in U(VI) as quickly as in the chemical nonequilibrium model. Lower concentrations result for the physical nonequilibrium model, especially where desorption rates are strongest, i.e., at the initial plume fringe. However, when the river water moves further into the aquifer soon equilibrium is reached and U(VI) concentrations become the same for both the chemical and physical nonequilibrium model, except for the leading edge of the river water. Here, U(VI) concentrations are noticeably decreased for the physical nonequilibrium model as compared to the chemical nonequilibrium model (days 216, 240, and 264 in Figure 7). This is the same effect that was observed in the column scenarios where the amplified adsorption strength in the immobile domains at early times of river water exposure temporally suppresses mass transfer to the mobile pore water.

[43] While the differences between chemical and physical nonequilibrium models are rather small with respect to the U(VI) concentrations and their dynamics, the U(VI) mass flux into the river in scenario F2 was more strongly affected by the choice of the model approach (Figure 8). The mass flux was noticeably higher for the physical nonequilibrium model in scenario F2. In contrast, the U(VI) mass flux in scenario F3 was quite similar for the two model approaches (Figure 8). The initial plume in scenario F3 was located next to the river. Therefore the development of a plume fringe and associated concentration gradients is less pronounced than in scenario F2, where the initial U(VI)-free zone between the plume and the river is strongly affected by the dispersive spreading of the plume. Adsorption disequilibrium is stronger at the plume fringes than at the plume center. Consequently, adsorption at the river boundary is closer to equilibrium in scenario F3 than scenario F2. Thus, U(VI)

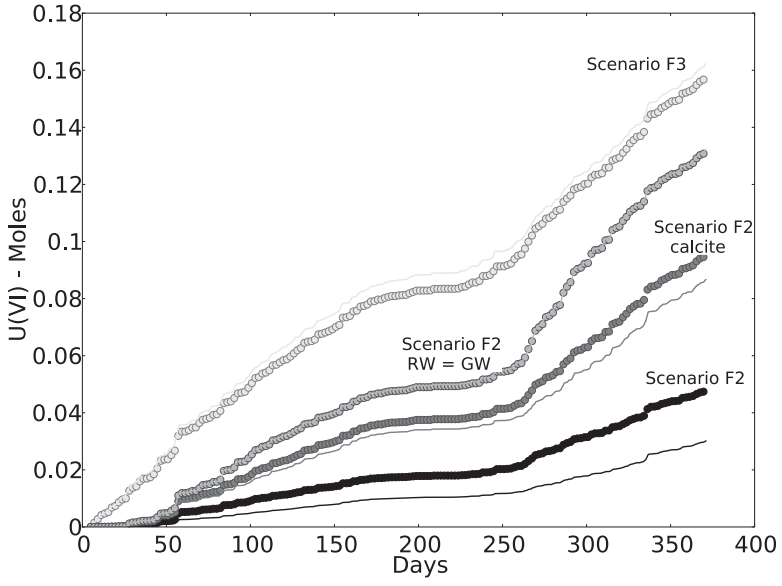

Figure 8. Mass of U(VI) discharged from the l-D model domain into the river for chemical (solid lines) and the physical nonequilibrium model (circles). Scenario F2 is indicated by the black color, scenario F2 with calcite dissolution is indicated by the second darkest color. Scenario F2 where the river water was set to groundwater quality (RW = GW) is indicated by the second lightest color. Scenario F3 is indicated by the lightest color.

discharge to the river in scenario F3 was less affected by mass transfer. A similar finding was reported by *Hammond and Lichtner* [2010] for this plume condition. As the differences in the behavior of the physical and chemical nonequilibrium model become increasingly pronounced with greater adsorption disequilibrium, the difference in U(VI) mass discharge between the two model approaches was higher in scenario F2 than in scenario F3. The mass discharge for the physical model in scenario F3 was lower than for the chemical model, which contrasts with the results from scenario F2. This is because the mass flux in scenario F3 was controlled by desorption rather than adsorption of U(VI) since the initial plume is located next to the river.

[44] While it appears that the two modeling approaches generate noticeable differences in U(VI) mass flux under scenario F2, it is not yet clear whether other factors could equally or even more strongly impact the mass discharge. Other important factors are, for example, the choice of surface complexation model, buffering reactions, or the river water composition and its variability. Two additional simulations for scenario F2 were carried out to reveal the impact of (1) calcite dissolution in the groundwater–river water mixing zone and (2) river water chemistry by setting the river water composition to that of groundwater. U(VI) mass-discharge increased when calcite dissolution by river water was allowed (Figure 8). The overall difference in mass flux between the calcite and no-calcite case was higher than the discrepancy between the physical and chemical nonequilibrium models for the individual cases (Figure 8). Furthermore, the difference between the physical and chemical models was less pronounced in the calcite case. Calcite dissolution increased the pH as well as the carbonate and calcium concentrations in the intruded river water and reduced the K_d and brings it closer to that of groundwater. As expected from the column simulations, no differences in U(VI) mass flux were observed between the physical and chemical models for the constant hydrochemistry simulation (river water = groundwater) because the K_d was constant. The constant hydrochemistry simulation, however, produces a higher mass flux than the variable hydrochemistry and the calcite case. Thus, accurate information on calcite distribution and river water composition appear to be more important for prediction of U(VI) discharge than the choice of the nonequilibrium model. The high importance of accurate information about processes affecting the major ion chemistry and their dynamics to predict U(VI) transport was also concluded in the work of *Yin et al.* [2011].

[45] As the net groundwater flow points toward the river, it is expected that adsorption sites between the initial plume and the river in scenario F2 will become increasingly occupied with simulation time, and that the distinct fringe zone conditions at this location will disappear. With time, scenario F2 should therefore slowly transform into scenario F3 and the discrepancy in U(VI) mass flux between the physical and chemical nonequilibrium models should diminish. However, even a 5 year simulation for scenario F2 did not show this effect. After 5 years the discrepancy in U(VI) mass discharge still shows a constant increase (Figure 9).

[46] Even if the discrepancy in U(VI) mass flux between the two model approaches may decrease at some stage, it might increase again when the trailing fringe of the plume and the associated adsorption disequilibrium reaches the groundwater–river water mixing zone near the river. That U(VI) mass discharge becomes increasingly sensitive to the kinetic sorption rates in the later stages of the plume migration was demonstrated by *Hammond and Lichtner* [2010] and indicates an increasing degree of adsorption disequilibrium. A demonstration of the expected differences in U(VI) mass discharge between the chemical and physical nonequilibrium models in the later stages of the plume

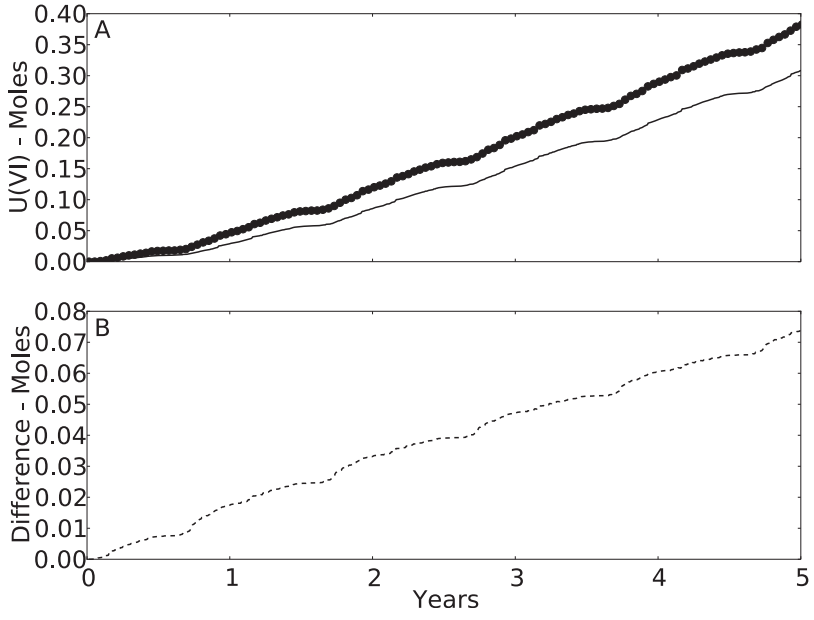

Figure 9. 5 year field scale simulation of scenario F2. (a) Mass of U(VI) discharged from the l-D model domain into the river for chemical (solid lines) and the physical nonequilibrium model (circles). (b) Absolute difference of U(VI) mass discharged between chemical and physical nonequilibrium model.

migration was beyond the scope of our investigation as the computational demand of the long-term field scale simulations was excessively large in the case of the physical nonequilibrium model. While the computation time of the 1 year field scale simulation was approximately 30 min with 8 CPUs of a clock speed of 2.8 GHz for the chemical nonequilibrium model, it was 4 days, i.e., 192 times more for the physical nonequilibrium model.

4. Conclusions

[47] Two alternative model approaches were compared that describe coupled intragrain diffusion and surface complexation of U(VI). Comparative model simulations were performed to investigate the behavior of these approaches for different reactive transport scenarios under both laboratory and field scale hydrological and hydrochemical conditions that were representative of, but not limited to, the Hanford 300A site. The physical nonequilibrium approach was found to be more sensitive to changes in water composition than the chemical nonequilibrium approach. The differences between these two approaches were increased with an increase in adsorption disequilibrium. On the other hand, the models behaved similarly when the system was closer to equilibrium and/or the changes in water composition were small. The effect of changing water composition was found to be significant in the unidirectional column scenarios as a result of sustained adsorption disequilibrium. Robust datasets from future column experiments are needed to confirm these findings.

[48] The differences in simulated plume behavior for the physical and chemical nonequilibrium models were not significant for Hanford 300A field scale conditions. Frequent groundwater flow reversals lead to less pronounced disequilibrium, especially near the plume center. On the other hand, the simulated discharge of U(VI) into the river was notably affected by the model approach due to the enhanced adsorption disequilibrium in the plume fringe located next to the river. However, this study shows that accurate knowledge of other variables, e.g., the distribution and concentration of calcite in the groundwater–river water interaction zone, or the variability in river water composition may be more important for an adequate prediction of the U(VI) mass discharge than the choice of the nonequilibrium approach. Furthermore, facies-scale physical and chemical heterogeneity, which has not been considered in the presented one-dimensional scenarios, may further diminish the significance of behavioral differences between the chemical and physical models under varying hydrochemistry. The adsorption site and adsorbed U(VI) concentrations are typically higher in finer grained aquifer facies [*Liu et al.*, 2008] where the advective velocity is lower than in more permeable zones. The physical and chemical models are expected to perform equally well for this condition as disequilibrium between the bulk and intragrain pore water may not be pronounced in these regions. The same is expected for the vadose zone of this site, as sorption disequilibrium was found to be small due to the long transport times in this zone [*Yabusaki et al.*, 2008]. It may be concluded that for field scale simulations of U(VI) transport at the Hanford 300A site the chemical nonequilibrium model, i.e., the multirate kinetic surface complexation model proposed by *Liu et al.* [2008], is a robust simplification of the diffusion-limited nonequilibrium approach while being computationally more efficient with fewer parameters. Although the differences in simulation results between the chemical nonequilibrium model and the physical nonequilibrium model were arguably small relative to the impact of other uncertainties at the Hanford 300A field site, this work demonstrates that the adequacy of the chemical model as an approximation to the physical model is highly dependent on the prevailing hydrochemical and hydrological conditions. Thus, with respect to other field sites and settings, it is recommended to evaluate the choice of the physical or chemical nonequilibrium approach on a case-by-case basis.

[49] **Acknowledgments.** We very much thank Aaron McDonough for preparing the parallel version of PHT3D, National Computational Infrastructure (NCI) Facility of Australia and iVEC, Western Australia, as well as Richard Silberstein (CSIRO) for providing high performance computing resources. This research was supported by a CSIRO OCE postdoctoral fellowship for JG; and by the US Department of Energy, Office of Biological and Environmental Research (BER) Subsurface Biogeochemistry Research Program (SBR) through the Hanford Integrated Field Research Challenge.

References

Bond, D. L., J. A. Davis, and J. M. Zachara (2008), Uranium(VI) release from contaminated vadose zone sediments: Estimation of potential contributions from dissolution and desorption, in *Adsorption of Metals to Geomedia II*, edited by M. O. Barnett and D. B. Kent, Chap. 14, pp. 375–416, Elsevier, Amsterdam, Netherlands.

Chen, W., and R. J. Wagenet (1995), Solute transport in porous media with sorption-site heterogeneity, *Environ. Sci. Technol.*, *29*, 2725–2734.

Connaughton, D. F., J. R. Stedinger, L. W. Lion, and M. L. Shuler (1993), Description of time-varying desorption kinetics: Release of naphthalene from contaminated soils, *Environ. Sci. Technol.*, *27*, 2397–2403.

Culver, T. B., S. P. Hallisey, D. Sahoo, J. J. Deitsch, and J. A. Smith (1997), Modeling the desorption of organic contaminants from long-term contaminated soil using distributed mass transfer rates, *Environ. Sci. Technol.*, *31*, 1581–1588.

Curtis, G. P., J. A. Davis, and D. L. Naftz (2006), Simulation of reactive transport of uranium (VI) in groundwater with variable chemical conditions, *Water Resour. Res.*, *42*, W04404, doi:10.1029/2005WR003979.

Davis, J. A., D. E. Meece, M. Kohler, and G. P. Curtis (2004), Approaches to surface complexation modeling of uranium (VI) adsorption on aquifer sediments, *Geochim. Cosmochim. Acta*, *68*(18), 3621–3641.

Donado, L. D., X. Sanchez-Vila, M. Dentz, J. Carrera, and D. Bolster (2009), Multicomponent reactive transport in multicontinuum media, *Water Resour. Res.*, *45*, W11402, doi:10.1029/2008WR006823.

Grenthe, I., J. Fuger, R. J. M. Konings, R. J. Lemire, A. B. Muller, C. Nguyen-Trung, and H. Wanner (1992), *Chemical Thermodynamics of Uranium*, 715 pp., Elsevier, New York.

Greskowiak, J., H. Prommer, C. Liu, V. E. A. Post, R. Ma, C. Zheng, and J. M. Zachara (2010), Comparison of parameter sensitivities between a laboratory and field scale model of uranium transport in a dual domain, distributed-rate reactive system, *Water Resour. Res.*, *46*, W09509, doi:10.1029/2009WR008781.

Grossl, P. R., M. Eick, D. L. Sparks, S. Goldberg, and C. C. Ainsworth (1997), Arsenate and chromate retention mechanisms on goethite. 2. Kinetic evaluation using a pressure-jump relaxation technique, *Environ. Sci. Technol.*, *31*(2), 321–326.

Haggerty, R., and S. M. Gorelick (1995), Multiple-rate mass transfer for modelling diffusion and surface reactions in media with pore scale heterogeneity, *Water Resour. Res.*, *31*(10), 2383–2400, doi:10.1029/95WR01583.

Haggerty, R., and S. M. Gorelick (1998), Modeling mass transfer processes in soil columns with pore-scale heterogeneity, *Soil Sci. Soc. Am. J.*, *62*, 62–74.

Haggerty, R., S. A. McKenna, and L. C. Meigs (2000), On the late-time behaviour of tracer test breakthrough curves, *Water Resour. Res.*, *36*(12), 3467–3479, doi:10.1029/2000WR900214.

Hammond, G. E., and P. C. Lichtner (2010), Field-scale model for the natural attenuation of uranium at the Hanford 300 Area using high-performance computing, *Water Resour. Res.*, *46*, W09527, doi:10.1029/2009WR008819.

Harbaugh, A. W., E. R. Banta, M. C. Hill, and M. G. McDonald (2000), MODFLOW-2000, the U.S. Geological Survey modular ground-water model—User guide to modularization concepts and the Ground-Water Flow Process, U.S. Geological Survey Open-File Report 00-92, 121 pp.

Ilton, E. S., N. P. Qafoku, C. Liu, D. A. Moore, and J. M. Zachara (2008), Advective removal of intraparticle uranium from contaminated vadose zone sediments, Hanford, U.S., *Environ. Sci. Technol.*, *42*, 1565–1571.

Kohler, M., G. P. Curtis, D. B. Kent, and J. A. Davis (1996), Experimental investigation and modeling of uranium(VI) transport under variable chemical conditions, *Water Resour. Res.*, *32*(12), 3539–3551, doi:10.1029/95WR02815.

Liu, C., J. M. Zachara, W. Yantasee, P. D. Majors, and J. P. McKinley (2006), Microscopic reactive diffusion of uranium contaminated sediments at Hanford, United States, *Water Resour. Res.*, *42*, W12420, doi:10.1029/2006WR005031.

Liu, C., J. M. Zachara, N. P. Qafoku, and Z. Wang (2008), Scale-dependent desorption of uranium from contaminated subsurface sediments, *Water Resour. Res.*, *44*, W08413, doi:10.1029/2007WR006478.

Liu, C., S. Shi, and J. M. Zachara (2009a), Kinetics of uranium (VI) desorption from contaminated sediments: Effect of geochemical conditions and model evaluation, *Environ. Sci. Technol.*, *43*, 6560–6566.

Liu, C., J. M. Zachara, L. Zhong, S. Heald, Z. Wang, B.-H. Jeon, and J. K. Fredrickson (2009b), Microbial reduction of intragrain U(VI) in contaminated sediment, *Environ. Sci. Technol.*, *43*, 4928–4933.

Ma, R., C. Zheng, H. Prommer, J. Greskowiak, C. Liu, J. Zachara, and M. Rockhold (2010), A field-scale reactive transport model for U(VI) migration influenced by coupled multi-rate mass transfer and surface complexation reactions, *Water Resour. Res.*, *46*, W05509, doi:10.1029/2009WR008168.

Nkedi-Kizza, P., W. Biggar, H. M. Selim, M. Th. van Genuchten, P. J. Wierenga, J. M. Davidson, and D. R. Nielsen (1984), On the equivalence of two conceptual models for describing ion exchange during transport through an aggregated oxisol, *Water Resour. Res.*, *20*(8), 1123–1130, doi:10.1029/WR020i008p01123.

Parkhurst, D., and C. A. J. Appelo (1999), User's guide to PHREEQC (Version 2)—A computer program for speciation, batch-reaction, one-dimensional transport, and inverse geochemical calculations, U.S. Geol. Surv. Water Resour. Invest. Rep. 99-4259.

Pedit, J. A., and C. T. Miller (1994), Heterogeneous sorption processes in subsurface systems. 1. Model formulations and applications, *Environ. Sci. Technol.*, *28*, 2094–2104.

Prommer, H., D. A. Barry, and C. Zheng (2003), MODFLOW/MT3DMS based reactive multicomponent transport modelling. *Ground Water*, *41*(2), 247–257.

Qafoku, N. P., J. M. Zachara, C. Liu, P. L. Gassman, O. S. Qafoku, and S. C. Smith (2005), Kinetic desorption and sorption of U(VI) during reactive transport in a contaminated Hanford sediment, *Environ. Sci. Technol.*, *39*(9), 3157–3165.

Stubbs, J. E., L. A. Veblen, D. C. Elbert, J. M. Zachara, J. A. Davis, and D. R. Veblen (2009), Newly recognized hosts for uranium in the Hanford Site vadose zone, *Geochim. Cosmochim. Acta*, *73*, 1563–1576.

Valocchi, A. J. (1985), Validity of the local equilibrium assumption for modelling sorbing solute transport through homogeneous soils, *Water Resour. Res.*, *21*(6), 808–820, doi:10.1029/WR021i006p00808.

Wang, P. P., C. Zheng, and S. M. Gorelick (2005), A general solution approach to advective-dispersive transport with multirate mass transfer, *Adv. Water Resour.*, *28*, 33–42.

Williams, B. A., C. F. Brown, W. Um, M. J. Nimmons, R. E. Peterson, B. N. Bjornstad, D. C. Lanigan, R. J. Serne, F. A. Spane, and M. L. Rockhold (2007), *Limited Field Investigation Report for Uranium Contamination in the 300 Area, 300-FF-5 Operable Unit, Hanford Site, PNNL-16435*, Pacific Northwest National Laboratory, Richland, Washington.

Willmann, M., J. Carrera, X. Sanchez-Vila, O. Silva, and M. Dentz (2010), Coupling of mass transfer and reactive transport for nonlinear reactions in heterogeneous media, *Water Resour. Res.*, *46*, W07512, doi:10.1029/2009WR007739.

Yabusaki, S. B., Y. Fang, and S. R. Waichler (2008), Building conceptual models of field-scale uranium reactive transport in a dynamic vadose zone-aquifer-river system, *Water Resour. Res.*, *44*, W12403, doi:10.1029/2007WR006617.

Yin, J., R. Haggerty, D. L. Stoliker, D. B. Kent, J. D. Istok, J. Greskowiak, and J. M. Zachara (2011), Transient groundwater chemistry near a river: Effects on U(VI) transport in laboratory column experiments, *Water Resour. Res.*, *47*, W04502, doi:10.1029/2010WR009369.

Zheng, C., and G. D. Bennett (2002), *Applied Contaminant Transport Modeling*, 2nd ed., Wiley, New York.

Zheng, C., and P. P. Wang (1999), *MT3DMS, A modular three-dimensional multi-species transport model for simulation of advection, dispersion and chemical reactions of contaminants in groundwater systems; documentation and user's guide*, U.S. Army Engineer Research and Development Center Contract Report SERDP-99-1, Vicksburg, MS, 202 pp.

J. A. Davis and M. B. Hay, U.S. Geological Survey, Menlo Park, CA 94025, USA.

J. Greskowiak, Working Group Hydrogeology and Landscape Hydrology, Institute for Biology and Environmental Sciences, Carl von Ossietzky University of Oldenburg, PO Box 2503, D-26111 Oldenburg, Germany. (janek.greskowiak@uni-oldenburg.de)

C. Liu and J. M. Zachara, Pacific Northwest National Laboratory, Richland, WA 99354, USA.

R. Ma and C. Zheng, Department of Geological Sciences, University of Alabama, Tuscaloosa, AL 35487, USA.

V. E. A. Post, Flinders University, Adelaide, Australia.

H. Prommer, School of Earth and Environment, University of Western Australia, Crawley, WA 6009, Western Australia.